Revealing Invisible Photonic Inscriptions: Images from Strain

Tao Ding,*[†,‡] Guoshuai Cao,[§] Christian G. Schäfer,[∥] Qibin Zhao,[†] Markus Gallei,[∥] Stoyan K. Smoukov,[‡] and Jeremy J. Baumberg*[†]

[†]Nanophotonics Centre, Cavendish Laboratory, University of Cambridge, CB3 0HE Cambridge, United Kingdom

[‡]Department of Materials Science and Metallurgy, University of Cambridge, 27 Charles Babbage Road, CB3 0FS Cambridge, United Kingdom
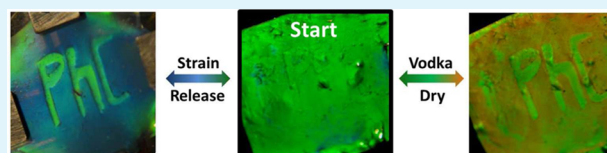
[§]Hushes Hall College, University of Cambridge, Wollaston Road, CB1 2EW Cambridge, United Kingdom

[∥]Ernst-Berl Institut für Technische und Makromolekulare Chemie, Technische Universität Darmstadt, Alarich-Weiss-Straße 4, 64287 Darmstadt, Germany

Ⓢ Supporting Information

ABSTRACT: Photonic structural materials have received intensive interest and have been strongly developed over the past few years for image displays, sensing, and anticounterfeit materials. Their "smartness" arises from their color responsivity to changes of environment, strain, or external fields. Here, we introduce a novel invisible photonic system that reveals encrypted images or characters by simply stretching, or immersing in solvents. This type of intriguing photonic material is composed of regularly arranged core−shell particles that are selectively cross-linked by UV irradiation, giving different strain response compared to un-cross-linked regions. The images reversibly appear and disappear when cycling the strain and releasing it. The unique advantages of this soft polymer opal system compared with other types of photonic gels are that it can be produced in roll to roll quantities, can be vigorously deformed to achieve strong color changes, and has no solvent evaporation issues because it is a photonic rubber system. We demonstrate potential applications together with a fabrication procedure which is straightforward and scalable, vital for user take-up. Our work deepens understanding of this rubbery photonic system based on core−shell nanospheres.

KEYWORDS: photonic crystals, tunable, strains, structural colors, patterns

■ INTRODUCTION

A traditional magic trick from premedieval times incorporates characters of invisible ink into secret documents using liquor or lemonade. Their security depends only on the recipient knowing how to reveal these characters on the paper. Such invisible inks are governed by chemical reactions that change the color of the pigments under certain conditions.[1] However, many such paper-based chemical inks degrade over time and cannot provide long-term storage of critical information.

Photonic crystals (PhCs), based on periodic arrangements of dielectric material, show vibrant structural color due to multiple scattering and interference. They have been widely used as colorants for image displays and sensors,[2−4] and are thus known as "photonic inks" (P-Inks). However, if such structural color images exhibit the same color as the surrounding paper, the invisible photonic patterns can be selectively revealed under appropriate conditions such as chemicals,[5] magnetic field,[6] or mechanical strains.[7] Because these photonic displays are composed of structural colors rather than pigment molecules, no photobleaching or degradation will occur and information can be safely stored on photonic paper over long periods. This type of photonic material is thus well-suited for anticounterfeit devices or the storage of secret information.

Current invisible photonic crystal patterns have been developed successfully to allow images to appear in several different ways, such as selective chemical wetting,[5] magnetic field manipulation,[6] and mechanical stretching.[7,8] More recently, gel-like photonic crystals (photonic gels) have been developed to deliver chemically or mechanically tunable photonic properties.[8−14] Initially the soft and cross-linked polymeric system consists of a periodically arranged lattice. Because the cross-linking degree is different between patterned and nonpatterned regions, spectral shifts of the structural colors are different under the same stimuli, which produces images with good contrast.[15,16] However, problems of solvent evaporation in the gels result in the loss of elasticity after longer times, which can lead to failure in both the invisibility and in the revealing processes for these invisible prints.

Recently, we have developed polymer opal films (POFs) made of ordered arrays of polystyrene core, poly(methylmethacrylate) interlayer, and poly(ethyl-acrylate) shell (PS@PMMA@PEA) nanospheres produced via a shear-ordering process (Supporting Information Figure S1).[17,18] The core/
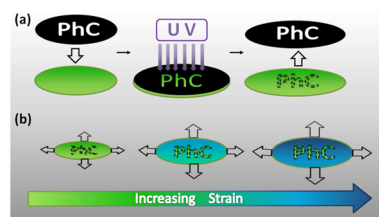
interlayer/shell polymer nanospheres are synthesized via emulsion polymerization on large scales (3 kg batches) for rapid production of the POFs. Because the elastic shells are made of PEA, the films can be easily bent,[19,20] stretched,[21−23] and imprinted[24] and possess robust mechanical strength even in the dried state.[25] These POFs behave as photonic rubbers that can be strongly tuned via stretching but still recover very well after release. Such rubber-like photonics are essentially different from the photonic gels and have unique advantages. First, the entire films are composed of polymeric colloidal crystal arrays (CCAs) rather than heterogeneous composites of CCA microcrystals or droplets, and thus show strong color intensities with fewer defects and less random interfacial scattering compared to previous reports. Second, they are mechanically robust without solvent loss issues since the elasticity does not depend on a gel system. Third, the polymer opal films are already scaled to kilogram batches for industry production,[26] which provides a solid basis for practical application of the invisible photonic prints for anticounterfeit and sensing devices.

In this Article, we use the POFs as a photonic paper with UV light as the writing pen. As shown in Scheme 1a, by selectively

Scheme 1. (a) "Writing" Invisible Photonic Patterns on POF and (b) Revealing the Invisible Patterns by Biaxial Stretching

irradiating certain parts of the POFs through a mask, characters or numbers are encrypted into the POFs though they cannot be seen by the naked eye. Because the UV irradiated regions are heavily cross-linked and more rigid, they develop less strain than nonirradiated regions under stretching. As a result little or no blue-shift of the structural color is observed in the irradiated regions compared with nonirradiated regions, which leads to strong color contrast between them (Scheme 1b). Stretching thus reveals the encrypted images. This invisible pattern technology has the unique advantage of easy fabrication (by UV irradiation) and easy examination (by manual stretching) compared with previous methods which applied magnets and chemicals.

EXPERIMENTAL SECTION

The PS@PMMA@PEA colloids were synthesized according to previous reports.[27] The polymer opal films were fabricated with a homemade roller rig as reported previously.[17] Typically, 2 g of PS@PMMA@PEA colloidal precursor along with benzophenone (as photoinitiator) were coextruded and rolled into thin films between two PET strips, and processed by a series of shear-ordering processes at 100 °C. The content of the benzophenone varied from 1, 5, and 10 wt % of the total amount of colloidal precursor. For long-term applications, extra photoinitiator in the shadowed regions can be diluted out by immersing the POFs in ethanol, which removes the chance of further cross-linking during repeated usage. The invisible patterns were written on the POFs via a UV lamp (wavelength 254 nm, 5 W, 5 cm above the POFs) through a black mask etched with certain characters. The overall thickness of the POF film is around 0.1

mm. The UV duration was adjusted from 30 min to 2 h. For the larger micropatterns, TEM grids were used as the mask for UV irradiation. The Poisson ratio of the material is between 0.4 and 0.5,[28] and it has an average refractive index of 1.52.[21,22] The elasticity modulus calculated from the stress−strain curves (Supporting Information Figure S2) is 0.015 N/mm^2 for the un-cross-linked film and 1.06 N/mm^2 for the cross-linked film. To reveal the patterns, the POFs were mounted on a homemade four-jaw stretching jig for biaxial stretching. Alternatively, the POFs could be immersed in alcohol for up to 1 min. The images of the POFs were taken with a Nikon camera. A halogen lamp (DH-2000, Ocean Optics) is used to probe the reflection spectra of the patterned and unpatterned regions of the film using multimode optical fibers coupled to a spectrometer (USB2000, Ocean Optics) (Supporting Information Figure S3). To observe the nanostructures of the POFs, the PS@PMMA@PEA nanospheres were stained with RuO_4 and cross-sectioned with focused ion beam (Zeiss). The SEM images of microstructures were recorded with a LEO 1530VP (Zeiss) at accelerating voltages of 5 kV.

RESULTS AND DISCUSSION

The entire POF films are doped with a photoinitiator (benzophenone). The UV light creates free radicals from benzophenone molecules, which further generate radicals within the PEA chains of the polymer matrix.[29] These radicals react to form covalent bonds between polymer chains, thereby cross-linking the polymer matrix.[30] Little variation of the reflection spectra between irradiated and nonirradiated regions is found, except for much longer time exposures which slightly red-shift the peak wavelength (by 10−20 nm). This red-shift is most likely due to the increase of the refractive index when polymer chains are cross-linked. Normally, the structural color of the POFs blue-shifts with increasing strain because the lattice separation decreases in the normal direction to the film surface.[22] However, the cross-linking in selected regions from UV irradiation produces different strains compared to regions that are not irradiated when they are under the same stress. The blue-shift of the reflection peak is not identical throughout the film, which results in color contrast of the images under stress. In order to apply the strain uniformly, we used biaxial stretching as shown in Figure 1a. As the applied strain increases, the invisible print "PhC" on the POFs became progressively clearer. The reflection spectra taken on non-irradiated regions blue-shift from 560 to 490 nm with increasing strain and recover back to 550 nm when the strain is released. On the other hand, the reflection taken on irradiated regions remains almost constant (at 580 nm) at different applied strains (Figure 1b,c). A small shoulder peak is observed (at 640 nm) for the cross-linked regions, which can be attributed to nonuniform cross-linking through the film depth. However, since its intensity is small compared to the main peak (580 nm), this nonuniformity has little influence on the optical appearance of the POFs. The reflection peak positions of the irradiated and nonirradiated regions are summarized in Figure 1d through one stretch−release cycle. Such stretch-and-release cycles are very reproducible (see Supporting Information Figure S4) with the peak positions summarized in Figure 1e. During each cycle, the entire POF is biaxially stretched by 12% and then released to its initial state. The peak positions of the irradiated regions remain constant throughout each cycle, while the reflection wavelength of nonirradiated regions shifts back and forth between 550 and 580 nm with good reproducibility. Such invisible patterns on POFs can reversibly appear and disappear even after 10 months storage at room temperature and ambient conditions (Supporting Information Figure S5).
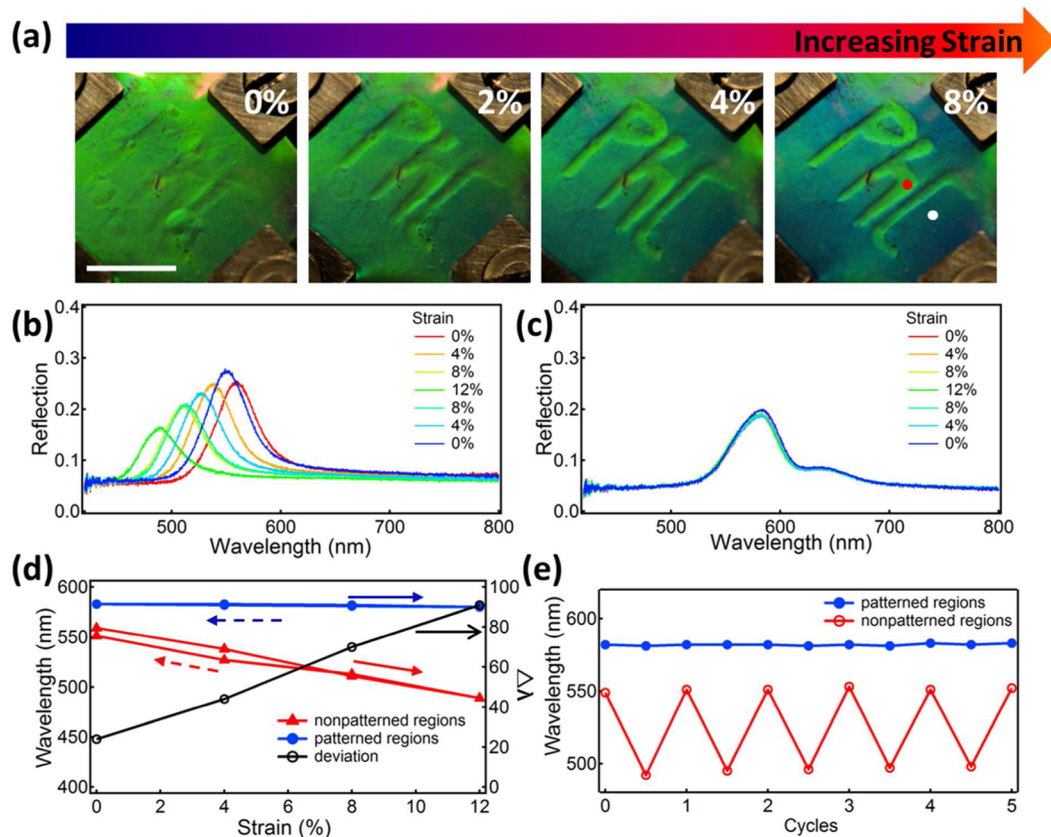
Figure 1. (a) Images of POFs (containing 10 wt % benzophenone, 2 h UV irradiation) with invisible patterns under different strains. Scale bar is 1 cm. White and red spots in the image represent the detection regions of reflection spectra taken in (b) nonirradiated and (c) irradiated regions under one strain−release cycle. (d) Changes of reflection wavelength with strains extracted from (b, red line) and (c, blue line). Black line is the difference of wavelength between these two regions. (e) Changes of reflection wavelength of irradiated and nonirradiated regions under 5 cycles of strain (12%) and release.
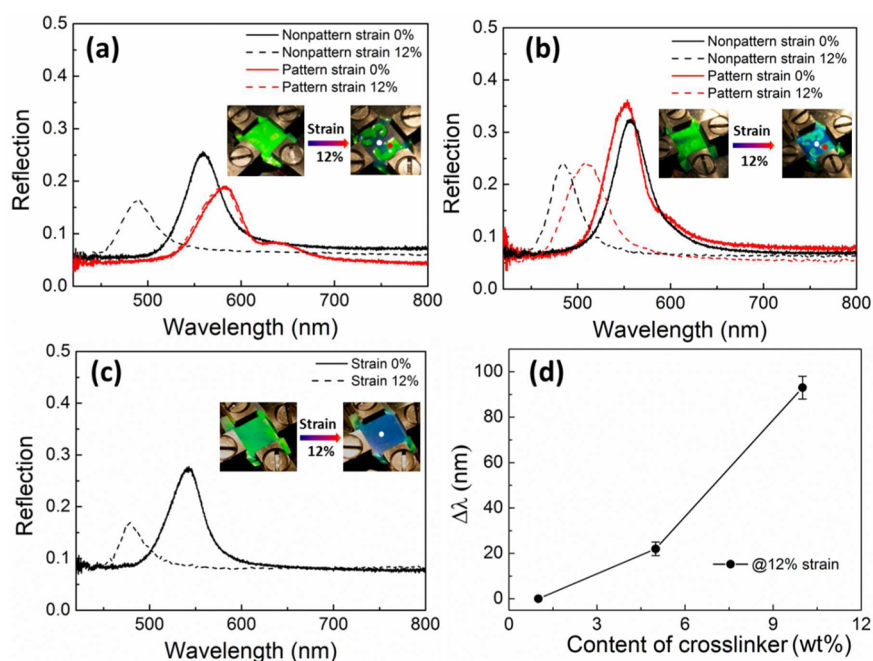

Figure 2. Reflection spectra of POFs containing different amount (wt %) of benzophenone (a) 10%, (b) 5%, (c) 1%. The invisible patterns were printed under 2 h UV irradiation. Insets are images of POFs before and after 12% strain. White and red spots show collection regions of the reflection spectra. (d) Difference of peak reflection wavelengths from irradiated and nonirradiated regions under 12% strain.
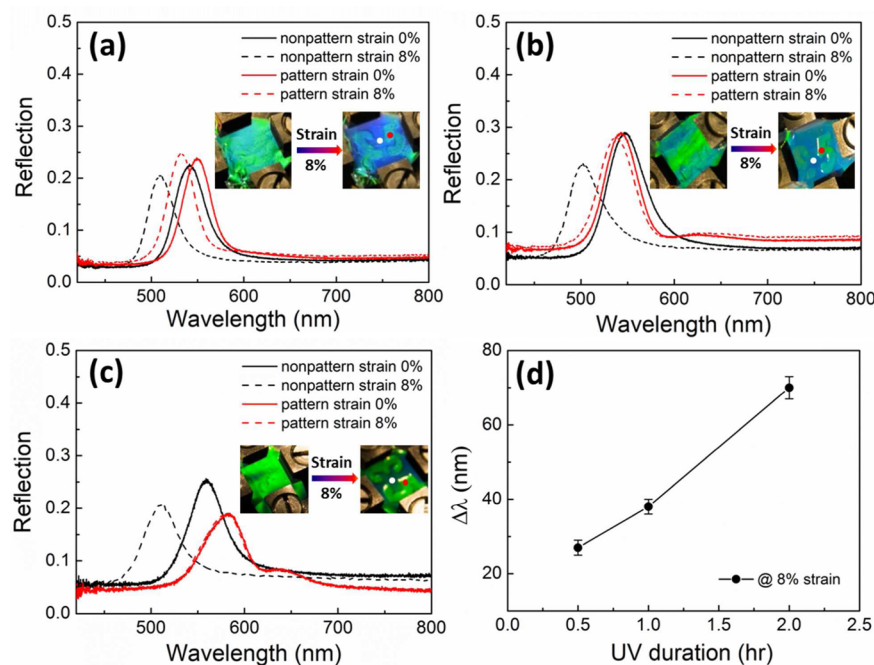
Figure 3. Reflection spectra of POFs (containing 10 wt % benzophenone) with invisible patterns printed under different duration of UV irradiation: (a) 0.5, (b) 1, (c) 2 h. Insets are the images of POFs before and after 8% applied strain. White and red spots show collection regions of the reflection spectra. (d) Difference of the peak reflection wavelength from irradiated and nonirradiated regions under 8% strain.

The difference in local strain between irradiated regions and nonirradiated regions under the same stress is critical for the appearance and disappearance of the invisible patterns. By engineering the local strains of the patterned regions, more diverse color patterns can be generated. Since the strain is dependent on the degree of cross-linking, which is correlated with how much photoinitiator is used and how long the UV irradiation is applied, we can fine-tune the different visual effects of the invisible patterns so that they will be more difficult to counterfeit.

As a demonstration, we write "£5" as an anticounterfeit bank note pattern. Different concentrations of photoinitiator at 1%, 5%, and 10% were used to fabricate POFs, followed by UV irradiation through a "£5" mask for 2 h. These were biaxially stretched to the same applied strain (12%), but they show different optical response (Figure 2). For POFs with 10% photoinitiator, the reflection spectra of the nonirradiated regions blue-shift from 559 to 489 nm while the irradiated regions remain at 581 nm. The large difference (up to 90 nm) of the peak reflection wavelengths between irradiated and nonirradiated regions means that the invisible images of "£5" are clearly observed at 12% strain (inset Figure 2a, Supporting Information video am5b02768_si_002.avi). For the POFs with 5% photoinitiator, however, the image contrast (inset of Figure 2b) is weaker (Supporting Information video am5b02768_-si_003.avi) because the reflection spectra of irradiated and nonirradiated regions blue-shift from 553 to 509 nm and 556 to 486 nm, respectively (Figure 2b), and the difference between the two peaks is only 20 nm (reflection spectra under different strains are shown in Supporting Information Figure S6). Further decreasing the photoinitiator to 1% results in no appearance of the image (inset Figure 2c, Supporting Information video am5b02768_si_004.avi) as the whole POF blue-shifts from 542 to 479 nm, and no difference between reflection spectra in irradiated and nonirradiated regions is seen. This progression of peak reflectivity difference (up to 90

nm at 10 wt %) between irradiated and nonirradiated regions at 12% strain with photoinitiator concentration is summarized in Figure 2d. Since full rigidity is obtained at 10 wt %, no further photoinitiator is of use.

The cross-linking dependence on irradiation time (0.5, 1, and 2 h) of the POFs at 10 wt % of photoinitiator shows the expected changes in optical response (at 8% applied strain in Figure 3). Short irradiation times give little contrast (inset Figure 3a), which progressively increases (Figure 3b) giving a peak wavelength difference now of 35 nm, until, for UV irradiation times of 2 h (Figure 3c), the wavelength difference reaches 70 nm (Figure 3d). This trend is again entirely consistent with high cross-linking for longer irradiation resulting in less local strain and less blue-shift of the structural color, producing strong color contrast of the images. However, longer UV times produce color contrast at 0% strain, and thus are not desirable in practice.

Larger area invisible micropatterns can be easily achieved, for instance here using a TEM grid as a photomask (Figure 4). On straining the sample, the irradiated region preserves green structural color while the shadowed regions blue-shift strongly.
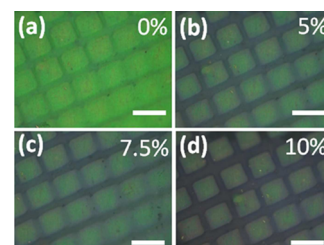

Figure 4. Optical images of micron-sized invisible patterns on POFs (10 wt % benzophenone, 2 h UV irradiation with TEM grid as mask) under different strains: (a) 0%, (b) 5%, (c) 7.5%, (d) 10%. Scale bars are 100 μm.
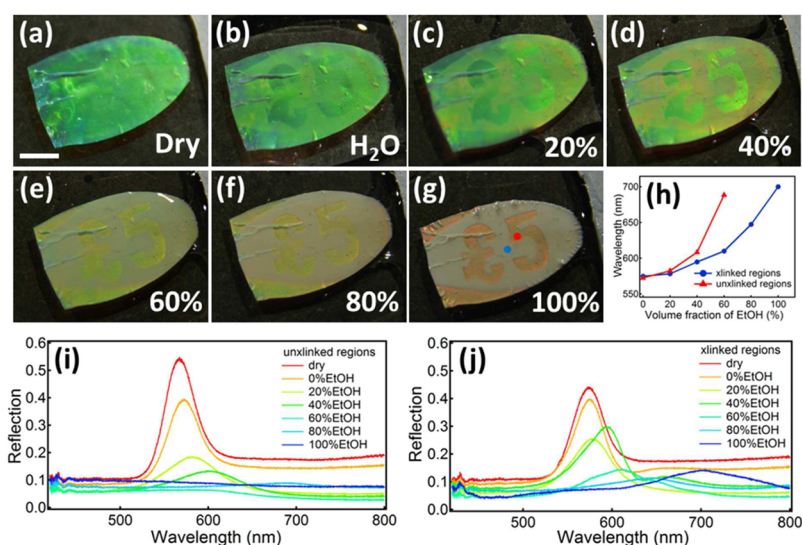
Figure 5. Photo images of POFs (containing 10 wt % benzophenone, 1 h UV irradiation of pattern) immersed in different media: (a) air (dried POFs), (b) water, and different mixtures of EtOH and H_2O, with (c) 20%, (d) 40%, (e) 60%, (f) 80%, (g) 100% of EtOH by volume fraction. Scale bar is 0.5 cm. Blue and red spots in part g show detection regions for the reflection spectra. (h) Wavelength of the reflection peak from irradiated (blue line) and nonirradiated (red line) regions when immersed in mixture of EtOH and H_2O with different volume fractions. (i, j) Reflection spectra of (i) nonirradiated regions and (j) irradiated regions after the POFs were immersed in different media.

As well as binary encoding, variable opacity UV masks can be used, allowing ranges of colors to be induced in different locations, allowing local rainbows to appear.

Although the POFs are dried rubber, they can also be wetted and swelled by specific solvents such as alcohols. Hence, different strains across cross-linked and stretchable regions can be produced by the osmotic pressure from the alcohol, so that the invisible photonic crystal patterns can be revealed. Different mixtures of ethanol (EtOH) and water are applied to swell the POFs, showing different effects revealing the invisible patterns on the POFs (Figure 5). With increasing volume ratio of EtOH, the colors of both irradiated and nonirradiated regions red-shift and the invisible patterns become more and more distinct compared to those from the dried POFs (Figure 5a–g). This red-shift is mainly due to the increase of lattice separation caused by solvent swelling, while the cross-linked polymer matrix prevents the matrix from swelling. This difference in swelling ratio on immersion thus generates different strains between irradiated and nonirradiated regions, and hence different color contrasts, with pure EtOH giving the best images. Moreover, the invisible pattern can show up within a few seconds when pure EtOH is the swelling agent, although it takes longer to recover to the original state as the EtOH has to evaporate out of the polymer matrix (Supporting Information Figure S7). Figure 4h summarizes the difference between (non)-cross-linked regions, which shows up to 15 nm separation when the volume fraction of EtOH reaches 40% (i.e., vodka). We also note that the nonirradiated regions appear pale since the reflection peak drops when the content of EtOH increases above 60% (see both images Figure 5e–g and reflection spectra in Figure 5i). This is because the EtOH partially enables spheres to move away from their equilibrium positions, melting the opal order. Figure 5i,j gives the corresponding reflection spectra of irradiated and nonirradiated regions when the POFs are immersed into different solvent mixtures. With increasing content of EtOH, both peaks indeed red-shift, but further in the nonirradiated regions. Because of the swelling induced disorder, the intensity of the peaks drops

to 10% in irradiated regions and vanishes for the nonirradiated regions. However, despite this, good contrast can still be observed in the images (Figure 5e–g). Such a responsive color change can thus not only be used for anticounterfeiting but also as a colorimetric indicator for ethanol sensing.

CONCLUSIONS

In conclusion, we have fabricated POFs with invisible patterns that can be revealed either by mechanical stretching or chemical swelling. The patterned regions are cross-linked with UV light through a mask so that they are more resistant to stretching and swelling compared with regions that are not cross-linked. When the POFs are stretched, the colors of cross-linked and non-cross-linked regions blue-shift to different extents so that strong contrast emerges revealing clear images on the POFs. Alternatively, swelling can result in different expansion of the patterned and nonpatterned regions so that different red-shifts result, improving the contrast and again revealing invisible patterns. With scalable fabrication of these POFs, such invisible photonic printing materials are well-suited for application in chemical sensing and anticounterfeit devices on bank notes and credit cards, document authentication, secret information encoding, and a variety of other opportunities.

ASSOCIATED CONTENT

ⓢ Supporting Information

SEM image of the cross-section of POFs, reflection spectra of irradiated and nonirradiated regions on POFs under many cycles of strain and release, and reflection spectra response to ethanol of the irradiated and nonirradiated regions. Videos demonstrating relevant properties. The Supporting Information is available free of charge on the ACS Publications website at DOI: 10.1021/acsami.5b02768.

AUTHOR INFORMATION

Corresponding Authors
*E-mail: dt413@cam.ac.uk.
*E-mail: jjb12@cam.ac.uk.

■ REFERENCES

(1) Macrakis, K.; Bell, E. K.; Perry, D. L.; Sweeder, R. D. Invisible Ink Revealed: Concept, Context, and Chemical Principles of "Cold War" Writing. *J. Chem. Educ.* **2012**, *89*, 529−532.

(2) Arsenault, A. C.; Puzzo, D. P.; Manners, I.; Ozin, G. A. Photonic-Crystal Full-Colour Displays. *Nat. Photonics* **2007**, *1*, 468−472.

(3) Kim, H.; Ge, J.; Kim, J.; Choi, S.-E.; Lee, H.; Lee, H.; Park, W.; Yin, Y.; Kwon, S. Structural Colour Printing Using a Magnetically Tunable and Lithographically Fixable Photonic Crystal. *Nat. Photonics* **2009**, *3*, 534−540.

(4) Yang, D.; Ye, S.; Ge, J. From Metastable Colloidal Crystalline Arrays to Fast Responsive Mechanochromic Photonic Gels: An Organic Gel for Deformation-Based Display Panels. *Adv. Funct. Mater.* **2014**, *24*, 3197−3205.

(5) Burgess, I. B.; Mishchenko, L.; Hatton, B. D.; Kolle, M.; Lončar, M.; Aizenberg, J. Encoding Complex Wettability Patterns in Chemically Functionalized 3D Photonic Crystals. *J. Am. Chem. Soc.* **2011**, *133*, 12430−12432.

(6) Hu, H.; Tang, J.; Zhong, H.; Xi, Z.; Chen, C.; Chen, Q. Invisible Photonic Printing: Computer Designing Graphics, UV Printing and Shown by a Magnetic Field. *Sci. Rep.* **2013**, *3*, 1484.

(7) Ye, S.; Fu, Q.; Ge, J. Invisible Photonic Prints Shown by Deformation. *Adv. Funct. Mater.* **2014**, *24*, 6430−6438.

(8) Jiang, P.; Smith, D. W.; Ballato, J. M.; Foulger, S. H. Multicolor Pattern Generation in Photonic Bandgap Composites. *Adv. Mater.* **2005**, *17*, 179−184.

(9) Yue, Y.; Kurokawa, T.; Haque, M. A.; Nakajima, T.; Nonoyama, T.; Li, X.; Kajiwara, I.; Gong, J. P. Mechano-Actuated Ultrafast Full-Colour Switching in Layered Photonic Hydrogels. *Nat. Commun.* **2014**, *5*, 4659.

(10) Chan, E. P.; Walish, J. J.; Urbas, A. M.; Thomas, E. L. Mechanochromic Photonic Gels. *Adv. Mater.* **2013**, *25*, 3934−3947.

(11) Chan, E. P.; Walish, J. J.; Thomas, E. L.; Stafford, C. M. Block Copolymer Photonic Gel for Mechanochromic Sensing. *Adv. Mater.* **2011**, *23*, 4702−4706.

(12) Chad, E.; Reese, A. V.; Mikhonin, M.; Kamenjicki, A.; Tikhonov; Asher, S. A. Nanogel Nanosecond Photonic Crystal Optical Switching. *J. Am. Chem. Soc.* **2004**, *126*, 1493−1496.

(13) Duan, L.; You, B.; Wu, L.; Chen, M. Facile Fabrication of Mechanochromic-Responsive Colloidal Crystal Films. *J. Colloid Interface Sci.* **2011**, *353*, 163−168.

(14) Yabu, H.; Nakanishi, T.; Hirai, Y.; Shimomura, M. Black Thin Layers Generate Strong Structural Colors: A Biomimetic Approach for Creating One-Dimensional (1D) Photonic Crystals. *J. Mater. Chem.* **2011**, *21*, 15154−15156.

(15) Xuan, R.; Ge, J. Invisible Photonic Prints Shown by Water. *J. Mater. Chem.* **2012**, *22*, 367−372.

(16) Wang, Z.; Zhang, J.; Xie, J.; Wang, Z.; Yin, Y.; Li, J.; Li, Y.; Liang, S.; Zhang, L.; Cui, L.; Zhang, H.; Yang, B. Polymer Bragg Stack as Color Tunable Photonic Paper. *J. Mater. Chem.* **2012**, *22*, 7887−7893.

(17) Finlayson, C. E.; Spahn, P.; Snoswell, D. R. E.; Yates, G.; Kontogeorgos, A.; Haines, A. I.; Hellmann, G. P.; Baumberg, J. J. 3D Bulk Ordering in Macroscopic Solid Opaline Films by Edge-Induced Rotational Shearing. *Adv. Mater.* **2011**, *23*, 1540−1544.

(18) Pursiainen, O. L. J.; Baumberg, J. J.; Winkler, H.; Viel, B.; Spahn, P.; Ruhl, T. Shear-Induced Organization in Flexible Polymer Opals. *Adv. Mater.* **2008**, *20*, 1484−1487.

(19) Finlayson, C. E.; Goddard, C.; Papachristodoulou, E.; Snoswell, D. R. E.; Kontogeorgos, A.; Spahn, P.; Hellmann, G. P.; Hess, O.; Baumberg, J. J. Ordering in Stretch-Tunable Polymeric Opal Fibers. *Opt. Express* **2011**, *19*, 3144−3154.

(20) Schäfer, C. G.; Lederle, C.; Zentel, K.; Stühn, B.; Gallei, M. Utilizing Stretch-Tunable Thermochromic Elastomeric Opal Films as Novel Reversible Switchable Photonic Materials. *Macromol. Rapid Commun.* **2014**, *35*, 1852−1860.

(21) Pursiainen, O. L. J.; Baumberg, J. J.; Ryan, K.; Bauer, J.; Winkler, H.; Viel, B.; Ruhl, T. Compact Strain-Sensitive Flexible Photonic Crystals for Sensors. *Appl. Phys. Lett.* **2005**, *87*, 101902.

(22) Kontogeorgos, A.; Snoswell, D. R. E.; Finlayson, C. E.; Baumberg, J. J.; Spahn, P.; Hellmann, G. P. Inducing Symmetry Breaking in Nanostructures: Anisotropic Stretch-Tuning Photonic Crystals. *Phys. Rev. Lett.* **2010**, *105*, 233909.

(23) Schäfer, C. G.; Gallei, M.; Zahn, J. T.; Engelhardt, J.; Hellmann, G. P.; Rehahn, M. Reversible Light-, Thermo-, and Mechano-Responsive Elastomeric Polymer Opal Films. *Chem. Mater.* **2013**, *25*, 2309−2318.

(24) Ding, T.; Zhao, Q.; Smoukov, S. K.; Baumberg, J. J. Selectively Patterning Polymer Opal Films Via Microimprint Lithography. *Adv. Opt. Mater.* **2014**, *2*, 1098−1104.

(25) Ito, T.; Katsura, C.; Sugimoto, H.; Nakanishi, E.; Inomata, K. Strain-Responsive Structural Colored Elastomers by Fixing Colloidal Crystal Assembly. *Langmuir* **2013**, *29*, 13951−13957.

(26) Finlayson, C. E.; Baumberg, J. J. Polymer Opals as Novel Photonic Materials. *Polym. Int.* **2013**, *62*, 1403−1407.

(27) Ruhl, T.; Spahn, P.; Winkler, H.; Hellmann, G. P. Large Area Monodomain Order in Colloidal Crystals. *Macromol. Chem. Phys.* **2004**, *205*, 1385−1393.

(28) Viel, B.; Ruhl, T.; Hellmann, G. P. Reversible Deformation of Opal Elastomers. *Chem. Mater.* **2007**, *19*, 5673−5679.

(29) Lin, A. A.; Sastri, V. R.; Tesoro, G.; Reiser, A.; Eachus, R. On the Crosslinking Mechanism of Benzophenone-Containing Polyimides. *Macromolecules* **1988**, *21*, 1165−1169.

(30) Schäfer, C. G.; Viel, B.; Hellmann, G. P.; Rehahn, M.; Gallei, M. Thermo-Cross-Linked Elastomeric Opal Films. *ACS Appl. Mater. Interfaces* **2013**, *5*, 10623−10632.